Comparing column dynamics in the liquid and vapor phase adsorption of biobutanol on an activated carbon monolith

Beckwée, Emile J.; Wittevrongel, Gille R.; Claessens, Benjamin

Published in:
Adsorption

DOI:
10.1007/s10450-022-00362-y

Publication date:
2022

License:
Other

Document Version:
Accepted author manuscript

Comparing column dynamics in the liquid and vapor phase adsorption of biobutanol on an activated carbon monolith

Emile J. Beckwée[†], Gille R. Wittevrongel[†], Benjamin Claessens*[†]

*corresponding author

benjamin.claessens@gmail.com

[†] Department of Chemical Engineering

Vrije Universiteit Brussel

Elsene

1050 Brussels

Belgium

Abstract

Adsorbent monoliths are gaining increasing interest in gas phase separation processes, but have rarely been studied for liquid phase separations. In this work, we investigate an activated carbon monolith for the recovery of biobutanol from model liquid mixtures as well as compare the obtained column dynamics with the adsorption of biobutanol from gas mixtures. Single solute adsorption isotherms of acetone, *n*-butanol and ethanol revealed the carbon's larger affinity for *n*-butanol (0.11 g/g adsorbed at 2 wt%), while dynamic separations on a fixed-bed of crushed monolith granules proved its capability to effectively separate an aqueous mixture of these three fermentation products. In contrast, liquid phase breakthrough experiments of *n*-butanol on the monolith column were marked by almost instantaneous detection of adsorbate at the outlet (< 5 min.) and broad tailing of the concentration curve. Measures to improve inlet flow distribution or increasing temperature to enhance mass transfer were unsuccessful. In contrast, using the same inlet flow distributors, a sharp breakthrough profile could be obtained in vapor phase, while the gas contact time (17 s) was much lower than in liquid phase (1300 s). A comparison of characteristic mass transfer times of the adsorption process highlighted the important role of the external film resistance in liquid compared to vapor phase adsorption.

Keywords: ABE fermentation, Biobutanol, Monolith, Activated carbon

1 Introduction

In recent years, increasing interest is going to the use of structured adsorbents (monoliths, foams, laminates, hollow fibers …) as opposed to a classical fixed-bed of spherical particles (Akhtar et al. 2014; DeWitt et al. 2018; Rezaei and Webley 2010). The use of such structured adsorbents allows the independent finetuning of heat, mass transfer and pressure drop characteristics of the adsorbent bed (Akhtar et al. 2014; DeWitt et al. 2018; Rezaei and Webley 2010). This has been shown to be especially important in gas phase separations. For instance, Rezaei *et al.* compared the performance of a packed bed of NaX beads and a NaX coated cordierite monolith in a three-step vacuum swing adsorption (VSA) cycle for CO_2 capture (Mosca et al. 2010). These authors showed that for short cycle times (15 s), the monoliths showed a higher recovery (80 %) and throughput (30 kg/m³ h) in comparison with the fixed bed (50 % recovery – 2.5 kg/m³ h throughput). The main cause for this increase in recovery and throughput being the much lower pressure drop. In another application, Li *et al.* reported 3-5 times faster pressurization steps compared to a fixed-bed of beads, when studying the use of a 5A zeolite for O_2 purification, due to a much lower pressure drop over the monoliths (Li et al. 1998). In a theoretical comparison of the heat and mass transfer properties of different structured adsorbents for CO_2 capture, Rezaei *et al.* showed that structured adsorbent beds outperform spherical beads, especially at high gas flow rates and short cycle times (Rezaei and Grahn 2012; Rezaei and Webley 2009).

The focus of most studies on adsorbent monoliths until now has been gas phase separations (Akhtar et al. 2014; DeWitt et al. 2018; Rezaei and Webley 2010). However, the use of monoliths could also be imagined beneficial for adsorption from the liquid phase. Firstly, a possible advantage could be the much easier draining of the column prior to thermal regeneration, removing the retained bulk liquid in the column. Secondly, when considering strong fouling feeds, less risk of clogging of the column could be expected when using

monoliths with a sufficiently large channel size. On the other hand, large differences in heat and mass transfer effects could be expected in liquid versus gas phase applications. Still, a comparison in dynamic breakthrough behavior on the same model separation case has not been reported in literature. In this work, we compare the adsorption column dynamics of the same monolith in liquid and vapor phase. As a model system, this paper focuses on the adsorptive recovery of biobutanol. Biobutanol is a renewable chemical, produced from biomass in a fermentation process and could potentially serve as in important feedstock for latex paint and rubber industry (Dürre 2007; Hahn et al. 2013; Jang et al. 2012; Kumar and Gayen 2011; Tashiro et al. 2013). In the so-called acetone-butanol-ethanol (ABE) fermentation process, *n*-butanol is the main product, with acetone and ethanol important side products (Dürre 2007; Hahn et al. 2013; Jang et al. 2012; Kumar and Gayen 2011). The traditional steam-stripping distillation process for the recovery and purification of biobutanol has a high energetic and economic cost (Abdehagh et al. 2014; Qureshi and Blaschek 2001), due to the low biobutanol concentrations in the fermentation broth (<2 wt%). Many alternatives have therefore been investigated and reviewed in literature (Abdehagh et al. 2014; Ibrahim et al. 2018; Kushwaha et al. 2019) of which adsorption is one of the most promising (Qureshi et al. 2005). The adsorptive recovery of biobutanol can be performed directly from the liquid fermentation broth (Abdehagh et al. 2017; Cousin-Saint-Remi et al. 2012; Faisal et al. 2016; Faisal et al. 2014; Gao et al. 2017; Gao et al. 2016; Groot and Luyben 1986; Jiao et al. 2015; Lee et al. 2016; Lin et al. 2013; Lin et al. 2012; Liu 2015; Maddox 1982; Nielsen and Prather 2009; Nielsen et al. 1988; Oudshoorn et al. 2009; Raganati et al. 2018; Saravanan et al. 2010; Staggs and Nielsen 2015; Wu et al. 2015; Xue et al. 2016; Yang et al. 1994) or from gasses produced during gas or vacuum stripping of the fermentation broth (Abdehagh et al. 2017; Bhattacharyya et al. 2017; Cao et al. 2015; Van der Perre et al. 2017). Of the different adsorbents screened in literature for biobutanol recovery hydrophobic materials such as MFI zeolites (Abdehagh et al. 2014;

Cousin-Saint-Remi et al. 2012; Maddox 1982; Milestone and Bibby 1983; Milestone and Bibby 1981), ZIF-8 (Cousin-Saint-Remi et al. 2012; Cousin-Saint-Remi et al. 2011; Gao et al. 2017) and activated carbon materials (Abdehagh et al. 2013; Cousin-Saint-Remi et al. 2012; Groot and Luyben 1986; Levario et al. 2012; Staggs et al. 2017; Weizmann et al. 1948; Xue et al. 2016) appear to be the most promising. The use of 3D-printed ZIF-8 monoliths for biobutanol recovery from vapor mixtures has been investigated by Denayer and coworkers (Claessens et al. 2020a; Lefevere et al. 2019). In one of the few articles focusing on liquid phase separations, Faisal *et al.* compared a steel monolith coated with silicalite-1 crystals with a fixed bed of silicalite-1 beads (Faisal et al. 2018). These authors showed that during the desorption process, a much higher purity could be obtained using the monolith (> 88.5 wt%), compared to silicalite-1 beads (> 69 wt%), due to the easier removal of entrained water. However, since the bulk density of the coated silicatlie-1 monolith was much lower than of the fixed-bed, the breakthrough times on the monolith (200 min), where much lower than for the beads (1000 min). Although activated carbons are promising adsorbents for biobutanol recovery (Abdehagh et al. 2013; Cousin-Saint-Remi et al. 2012; Groot and Luyben 1986; Levario et al. 2012; Staggs et al. 2017; Weizmann et al. 1948; Xue et al. 2016), activated carbons in structured form have not yet been studied for biobutanol recovery.

In this work, we investigate the adsorption of *n*-butanol on a commercial, extruded activated carbon monolith. To compare differences in vapor and liquid phase operation, the adsorption of *n*-butanol is studied from both phases in dynamic conditions. First, the adsorbent is characterized via SEM images and Ar and CO_2 porosimetry. Secondly, the liquid phase equilibrium of *n*-butanol was investigated via the measurement of adsorption isotherms. Thirdly, dynamic breakthrough curves of model mixture were measured on the activated carbon monolith and a fixed-bed of activated carbon particles. Finally, a comparison is made with vapor phase breakthrough curves on the same material.

2 Materials & Methods

2.1 Textural characterization

A commercially available extruded activated carbon monolith (Ingevity, North Charleston, South Carolina, USA), with a length of 15.0 cm, external diameter of 3.0 cm and mass of 48.26 g was used as adsorbent (Fig. 1). Scanning electron microscopy pictures were taken using a Jeol JCM-6000Plus (Akishima, Tokyo, Japan) applying an acceleration voltage of 10 kV. A side-by-side comparison of the cross sections of the monolith and a model is depicted in Fig. S1. Based on this model, the total volume of the channels $V_{channels}$ and total volume of the structure $V_{monolith}$ were obtained and used to calculate the external porosity ε, equivalent to the bed porosity for a fixed-bed of spheres (Eq. 1).

$$\varepsilon = \frac{V_{channels}}{V_{monolith}} \quad (1)$$

Fig 1. Side (A) and top view (B) image of the used activated carbon monolith, wrapped in heat shrink tubing

2.2 Internal porosity

The micro- and mesoporosity of the activated carbon was assessed by measuring Ar (-186 °C) and CO_2 (0 °C) physisorption on an Autosorb-1 device (Quantachrome Instruments, Odelzhausen, Germany). Prior to measurement of the isotherms, a small monolith sample was activated under vacuum at 150 °C for 8 h. Pore size distributions were derived from the Ar and CO_2 isotherms by the quenched solid density functional theory (QSDFT) and the non-local density functional theory (NLDFT), respectively. Macroporosity was evaluated by mercury

intrusion on a small sample of intact monolith, measured on a mercury Porosimeter 2000 (1-2000 bar) (Thermo Fisher Scientific, Waltham, Massachusetts, USA).

2.3 Single solute adsorption isotherms

Single solute adsorption isotherms of *n*-butanol, ethanol and acetone were constructed by use of the batch adsorption technique. An overview of the used adsorbates indicating supplier and purity is provided in Table S1. For each batch measurement, 200 mg of crushed adsorbent was added to a 10 mL vial and thermally regenerated overnight. The temperature was increased to 150 °C at a rate of 0.5 °C/min. Afterwards, the vials were rapidly capped. Once the adsorbent had cooled down to room temperature, 2 mL of an aqueous *n*-butanol, acetone or ethanol mixture was added. An equilibration time of 6 h was employed, after which the external liquid phases were removed, filtered with 0.2 µm polytetrafluoroethylene filters (Pall Corporation, Port Washington, New York, USA) and concentrations measured by use of an Agilent 7820A gas chromatograph. Subsequently, equilibrium adsorption capacities q_{eq} were calculated by Eq. 2 (Duerinck et al. 2011).

$$q_{eq} = \frac{x_0\, m_l - x_{eq}(m_l - \rho_{adsorbate}\, V_p\, m_{ads})}{m_{ads}} \quad (2)$$

In which x_0 is the initial mixture concentration (g/g), m_l is the mass of the added mixture (g), x_{eq} is the equilibrium concentration (g/g), $\rho_{adsorbate}$ is the adsorbed phase density (g/mL), V_p is the pore volume based on argon physisorption at -186 °C (mL/g) and m_{ads} is the mass of the thermally regenerated adsorbent (g). The adsorbed phase density was considered equal to the liquid phase density of the adsorbate, as is common in literature (Duerinck et al. 2011). Measurement errors were determined using classical error propagation formulas (Section S3) (Ku 1966).

2.4 Breakthrough experiments

Breakthrough experiments were performed using both liquid and vapor phase mixtures on the activated carbon monolith and on a fixed-bed of crushed and sieved carbon monolith particles.

2.4.1 Column packing

The packed bed column was constructed by packing 7.23 g of crushed monolith adsorbent in a 15.0 cm long, 1.0 cm internal diameter stainless-steel column, equipped with 0.5 μm filters at both ends. The packing was prepared by crushing a spare activated carbon monolith and sieving the crushed adsorbent to obtain particles within the range of 0.4 to 0.6 mm.

The monolith column was constructed by wrapping the monolith in heat shrink tubing (RS Components, Corby, United Kingdom) to prevent leakage of fluid through the outer wall. In- and outlet fittings were in-house machined from aluminum and placed at both ends of the monolith. A technical drawing of both fittings as well as a schematic view of the assembled monolith column are shown in Fig. S4. The fittings were held in place by tightening an aluminum nut on the outside thread of the fittings, thereby clamping Teflon and rubber rings. A conical inlet piece was printed by use of an Ultimaker 3 3D-printer (Ultimaker, Utrecht, The Netherlands) in polylactic acid (PLA), with the aim of reducing the volume in front and behind the monolith, as discussed further (Fig. S5). The total monolith column contained 48.26 g of activated carbon, with a length of 15.0 cm and 3.0 diameter.

2.4.2 Liquid phase breakthrough

Liquid phase breakthrough experiments were performed using an Integrated Lab Solutions setup (ILS, Berlin, Germany), of which an in-depth description is given by Duerinck *et al.* (Duerinck et al. 2011) and a schematic diagram depicted in Fig. S6. Before conducting a breakthrough experiment, the adsorbent was regenerated by flowing N_2 at 80 NmL/min through

the column, while increasing the temperature to 100 °C at 0.5 °C/min. Heating at 100 °C was maintained overnight to further desorb and displace adsorbate. For the breakthrough experiments, the adsorption column was first saturated with MilliQ water, at the same flow rate as used during the actual breakthrough experiment, to fill the column with water and stabilize the liquid flow through the system. Afterwards, a mixture of *n*-butanol/water or ABE/water, was fed. Analysis of the effluent was performed by collecting samples at a certain time interval and measuring the concentration by an Agilent 7820A gas chromatograph.

2.4.3 Vapor phase breakthrough

Vapor phase breakthrough experiment were performed on an in-house developed setup, described in detail in previous works (Claessens et al. 2021; Van der Perre et al. 2017) and depicted in Fig. S7. Briefly, an inert carrier gas is bubbled through an *n*-butanol containing evaporator. By fixing the evaporator temperature and extra dilution with carrier gas, the *n*-butanol vapor pressure can be finetuned. The carrier gas and adsorbate vapor is then sent through the monolith column, detection at the column outlet is performed by online sampling with a gas chromatograph (HP 6890, Agilent). Prior to performing an adsorption experiment, the monolith was activated by heating with an inert carrier (He) at 0.5 °C / min to 100 °C, holding this temperature overnight.

2.4.4 Analysis.

The adsorption capacity of an adsorbate was calculated by equation 3, derived from a mass balance over the adsorption column (Duerinck et al. 2011).

$$q_i = \left(\frac{v\,(\tau_{ads,i} - t_{dead})}{L} - 1\right)\frac{\varepsilon\, x_{i,in}\, \rho_l\, V}{m_{ads}} \qquad (3)$$

With q_i the adsorption capacity of adsorbate i (g/g), v the interstitial velocity (cm/s), $\tau_{ads,i}$ the average breakthrough time of adsorbate i (s), t_{dead} the dead time of the setup (s), L the length of the column (cm), $x_{i,in}$ the concentration of the feed mixture (g/g), ρ_l the feed mixture density (g/cm^3) and V the volume of the column (cm^3).

From blank breakthrough experiments, the dead volumes of the liquid and vapor phase breakthrough setups were determined to be 2.1 mL and 3.5 mL, respectively. The average breakthrough time for adsorption, i.e. the first moment of the adsorption breakthrough curve, can be calculated by following equation:

$$\tau_{ads,i} = \int_0^\infty \left(1 - \frac{x_{i,out}(t)}{x_{i,in}}\right) dt \tag{4}$$

In which $x_{i,out}(t)$ is the concentration at the column outlet at time t (g/g). The adsorption selectivity of component i over component j can be calculated by following equation:

$$\alpha_{i,j} = \frac{\frac{q_i}{q_j}}{\frac{x_i}{x_j}} \tag{5}$$

2.5 Estimation of mass transfer resistances

The liquid and vapor phase diffusion coefficients of *n*-butanol in water and helium were calculated using the Stokes-Einstein and Chapman-Enskog equations, respectively, (Poling et al. 2007) and are summarized in supporting information (Section S6).

To estimate the film mass transfer resistance, the Hawthorn equation was used (Hawthorn 1974):

$$Sh = \frac{d_h k_f}{D_m} = 2.95 \left(1 + 0.095\, Re\, Sc \frac{d_h}{L}\right)^{0.45} \tag{6}$$

With Sh the Sherwood number, d_h the hydraulic diameter (m), D_m the *n*-butanol molecular diffusivity (m^2/s), k_f the film mass transfer coefficient (m/s), L the monolith length (m), Re the Reynolds number and Sc the Schmidt number.

To estimate the relative contribution of the external film mass transfer resistance, compared to the internal mass transfer resistance, the characteristic timescales were estimated as follows.

$$t_{film} = \frac{\left(\frac{d_h}{2}\right)}{k_f} K \tag{7}$$

$$t_{wall} = \frac{\left(\frac{d_w}{2}\right)^2}{D_{macro}} \tag{8}$$

With d_w the wall thickness of the monolith channels (m) and K the dimensionless slope of the adsorption isotherm, derived from the liquid and vapor phase *n*-butanol adsorption isotherms, respectively (Fig. S8). In most gas-phase adsorption applications, macropore diffusion is the rate-limiting step (Kärger et al. 2012). We therefore estimated the internal diffusion coefficient D_{macro} via the liquid or gas phase diffusion coefficient and the dimensionless slope of the adsorption isotherm K (Eq. S11). These times were compared to the contact time of the carrier gas or liquid during breakthrough, defined as:

$$t_{contact} = \frac{V_{channels}}{F} \tag{9}$$

With F the volumetric flow rate (m^3/s). The relation between the contact time and the estimated characteristic mass transfer times is graphically represented Fig. S9.

3 Results & Discussion

3.1 Textural characterization

The commercial monolith used in this work consisted of square-shaped, parallel channels, of a size of 1.3 mm, as determined by SEM analysis (Fig. S2). The monolith walls had a thickness of 0.3 mm. From the obtained channel sizes and wall sizes, a bulk porosity of 0.6 was calculated (Eq. 1), making the external porosity of the monolith slightly larger than that of a fixed-bed of spherical particles (0.3 – 0.5, (Ruthven 1984)). Ar and CO_2 physisorption revealed the activated carbon monolith to be largely microporous, with 48 % of the pore volume being of pores < 2 nm. Within this region, the pore size distribution was quite broad, with distinct peaks at 0.4, 0.8 and 1.5 nm (Fig. S10). From Ar physisorption, a total pore volume of 0.29 ml/g (pore width 0.45-21.05 nm) was calculated, which is slightly smaller than two other granular activated carbons we recently identified to be good adsorbents to remove isobutanol from aqueous mixtures (F300 – 0.52 ml/g and F400 – 0.48 ml/g) (Claessens et al. 2020b). Mercury intrusion/extrusion showed a broad macropore size distribution between 0.05 and 0.52 µm, with a maximum at 0.31 µm, and resulted in a total pore volume of 0.29 cm^3/g (pore width 7.5 nm-100 µm) (Fig. S11). A summary of the textual properties of the monolith and total pore volume can be found in Table 1, while Hg intrusion, Ar and CO_2 physisorption isotherms, pore size distributions and a more in-depth overview of the micro-, meso- and macropore volumes, can be found in supporting information (Figs. S10 and S11, Table S4).

Table 1. Characteristic dimensions of the activated carbon monolith

Length (cm)	Diameter (cm)	Channel width (mm)	Wall thickness (mm)	Cell density (cpsi)	External porosity	Pore volume (Ar) (cm^3/g)	Pore volume (Hg) (cm^3/g)
15	3	1.3	0.3	242	0.6	0.29	0.29

3.2 Single solute adsorption isotherms

To investigate the affinity of the activated carbon monolith for different ABE mixture components, single solute isotherms of *n*-butanol, ethanol and acetone were measured (Fig. 2). The resulting *n*-butanol isotherm has a type I shape, with a saturation capacity of 0.11 g/g, reached at an *n*-butanol concentration typical for a fermentation broth (2 wt%). The obtained equilibrium capacity is slightly lower than reported in literature for granular activated carbon adsorbents (between 0.15 g/g and 0.51 g/g, (Abdehagh et al. 2013; Cousin-Saint-Remi et al. 2012; Groot and Luyben 1986; Levario et al. 2012; Staggs et al. 2017; Weizmann et al. 1948; Xue et al. 2016). Similarly, in a recent study, we observed equilibrium adsorbed amounts for isobutanol between 0.17 and 0.25 g/g in batch uptake experiments with a 2 wt% mixture on various activated carbons (Claessens et al. 2020b). However, looking at the isotherms of ethanol and acetone (Fig. 2), it can be observed that ethanol and acetone are adsorbed in lower amounts compared to *n*-butanol at the same concentration. Throughout the assessed concentration range, the equilibrium capacities of ethanol are the lowest of the three adsorbates, followed by acetone and then *n*-butanol. At acetone (1.0 wt%), *n*-butanol (2.0 wt%) and ethanol (0.3 wt%) concentrations typically found in fermentation broths (Dürre 2007; Hahn et al. 2013; Jang et al. 2012; Kumar and Gayen 2011), 0.11 g/g *n*-butanol is adsorbed, while only 0.05 g/g acetone and 0.01 g/g ethanol are adsorbed. Hence, the absolute *n*-butanol equilibrium capacity is slightly lower than reported for other carbons in literature. However, the adsorbed amount of *n*-butanol (0.11 g/g) at concentrations similar to that in the fermentation broth (2 wt%), is still higher than that of acetone (1.0 wt% - 0.05 g/g) and ethanol (0.3 wt% - 0.01 g/g), suggesting the monolith could be used to selectively adsorb *n*-butanol.

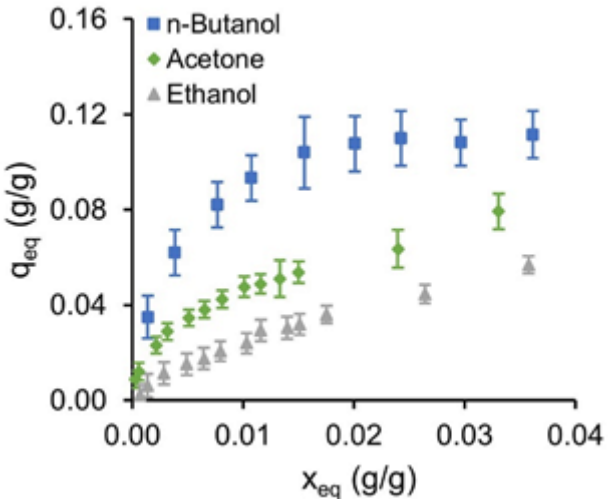

Fig. 2 Single solute adsorption isotherms of *n*-butanol, acetone and ethanol, diluted in water, on crushed monolith samples, measured at room temperature.

3.3 Dynamic separation on crushed monolith

To investigate whether the activated carbon is able to separate model ABE mixtures, dynamic breakthrough experiments were performed on a fixed-bed of crushed monolith granules (Fig. 3). Ethanol is the least retained component (τ_{ethanol} = 12.9 min), followed by acetone (τ_{acetone} = 13.2 min) and *n*-butanol ($\tau_{n-\text{butanol}}$ = 39.8 min). Both ethanol and acetone are adsorbed and subsequently displaced, as visible form their concentration profiles, which increase until 1.5 and 1.6 times the feed concentration respectively.

The adsorption capacities obtained from the dynamic separations of acetone, *n*-butanol and ethanol were 0.01 g/g, 0.10 g/g and < 0.01 g/g, respectively. The *n*-butanol adsorbed amount is close to that obtained from single solute isotherm measurements, with only traces of acetone and ethanol co-adsorbing. Although more acetone is co-adsorbed than ethanol, the *n*-butanol selectivity over these two components is almost the same, being 4.3 and 4.1 for ethanol and acetone, respectively This result confirms the carbon's affinity for *n*-butanol, then for acetone and finally for ethanol. The activated carbon thus appears to be able to selectively remove *n*-butanol from model ABE mixtures.

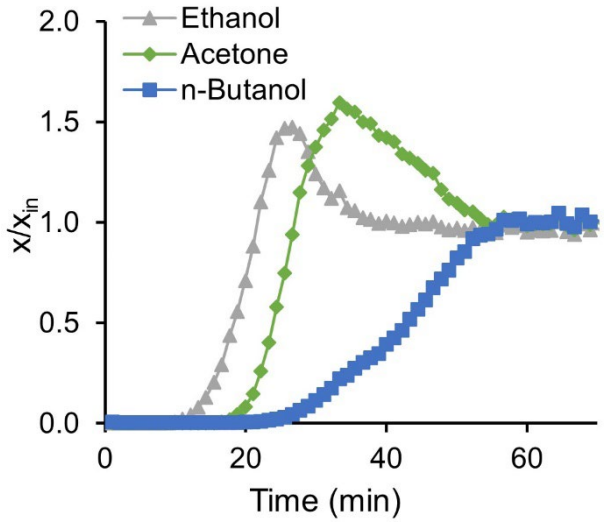

Fig. 3 Adsorption breakthrough curves of acetone (1.0 wt %), *n*-butanol (2.0 wt %) and ethanol (0.3 wt %) diluted in water, on a packed column of crushed monolith granules at a flowrate of 1.0 mL/min, measured at room temperature

3.4 Dynamic performance of the monolith column

Next, the performance of the adsorbent monolith was investigated in dynamic conditions, by performing a breakthrough experiment with an aqueous 2 wt% *n*-butanol mixture (Fig. 4a). Surprisingly, an almost instantaneous breakthrough of *n*-butanol was observed (after < 5 min.), followed by an extremely broad tail. Based on the single component isotherm (Fig. 2), an average breakthrough time of around 90 min. would be expected under these experimental conditions.

It was hypothesized that this early breakthrough could be caused by two effects. Firstly, flow maldistribution at the column inlet is known to have a major contribution to broadening of concentration profiles in gas phase breakthrough (Ahn and Brandani 2005; Crittenden et al. 2005; Sharma et al. 2020). Also, a small kink was visible in the breakthrough profile at x/x_{in} = 0.6, possibly indicating faster breakthrough through some of the monolith channels. In this first experiment (Fig. 4a), we kept a dead volume in front of the column inlet, which was not specifically designed to aid in distribution of the flow (Fig. S4). To improve flow distribution

at the column inlet, we investigated different alternatives (see further). Secondly, it was hypothesized that the broadening of the breakthrough curves was caused by mass transfer resistances, be it in the liquid phase or in the internal monolith walls. In an attempt to improve this, we performed a breakthrough experiment at higher temperature. It should, however, be highlighted that good breakthrough profiles were obtained on the packed column of crushed monolith (Fig. 3), at higher interstitial velocities (5.3x10-4 m/s) for the fixed-bed compared to the monolith (1.2x10-4 m/s). Hence, the fast breakthrough appears to be related to kinetic effects (mass transfer effects or flow distribution), rather than the fundamental affinity of the carbon material for n-butanol. Furthermore, the concentration entry length was calculated using a literature correlation and was proven to be much lower than the length of the monolith (Supporting Information – Section S10).

First, to improve flow distribution at the column inlet, we filled the inlet volume with a fixed-bed of glass beads, with two different particle diameters and repeated the breakthrough measurements (Fig. 4a and S5). Using this fixed-bed of inert beads at the column inlet let to a slight shift in initial breakthrough times (≈ 10 min.). Using smaller quartz beads led to a larger increase in breakthrough time. Hence, channeling effects appear to be slightly reduced by employing a fixed-bed in front of the column inlet. However, large tailing was still observed on the concentration profiles.

Next, to further reduce the dead volume at the column inlet, we 3D-printed a conical structure, with an initial diameter equal to the inlet tubing diameter and a final diameter equal to the full monolith diameter (Fig. S5). These 3D-printed conical inlet pieces were also filled with glass beads. Using this conical inlet piece let to no better or worse performance than when just using a fixed-bed of glass beads (Fig. 4b). Initial breakthrough times were comparable to those previously obtained with a fully empty cylindrical inlet piece (Fig. 4a). Hence, the extra

effect of inlet volume reduction by using this conical 3D-printed structures appears to be negligible.

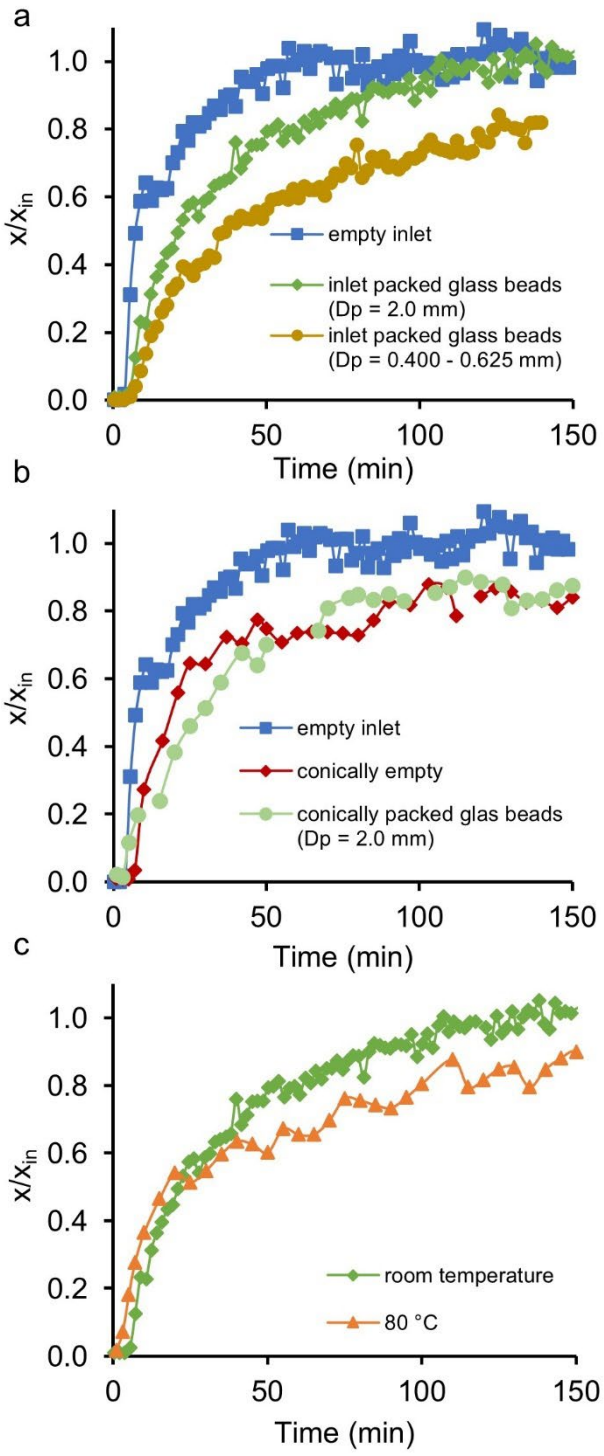

Fig. 4 Adsorption breakthrough curves at room temperature of a 2 wt% *n*-butanol mixture, diluted in water at a flow rate of 3.0 mL/min on the activated carbon monolith column. The empty inlet piece is compared with the inlet filled with a fixed bed of glass beads (a) and with a conically 3D-printed inlet piece (empty and filled with glass beads – b). A comparison between room temperature breakthrough and breakthrough at 80 °C is also shown (c)

Although a small improvement was obtained by using a fixed-bed of inert glass beads to improve flow distribution, still broad breakthrough profiles with large tailing were obtained. In a next step, we increased the experimental temperature to 80 °C, to improve both external and internal mass transfer. From the Stokes-Einstein equation (Eq. S4), it can be calculated that the *n*-butanol-water diffusion coefficient increases from 8.8 10^{-10} m²/s at room temperature to 3.0 10^{-9} m²/s at 80 °C. Still, on the resulting breakthrough profile, significant tailing could be observed (Fig. 4C), but again a small shift in average breakthrough time could be observed by increasing temperature. Hence, while putting a fixed-bed of glass beads at the column inlet and increasing temperature leads to a slight improvement in breakthrough performance, still large tailing was observed on the butanol profiles. Finally, conducting the breakthrough experiment at one tenth of the volumetric flowrate, still resulted in premature detection of n-butanol at the outlet (Fig. S12). It is therefore still unclear whether the observed broad breakthrough profiles were caused by mass transfer resistances or flow distribution effects.

3.5 Vapor-phase breakthrough

Since diffusion coefficients in gas phase conditions are typically 3 orders of magnitudes higher than in liquid phase, we wanted to investigate whether the observed mass transfer or flow maldistribution effects observed in liquid phase were also observed in vapor phase conditions. Therefore, a breakthrough experiment was performed on the same monolith column, but using *n*-butanol as a vapor diluted in He as carrier gas (Fig. 5). Surprisingly, a sharp *n*-butanol breakthrough profile was obtained, with an average breakthrough time of 19.5 h,

leading to an amount adsorbed of 0.177 g/g. The higher *n*-butanol uptake, compared to the saturation value obtained from the single solute isotherm (Fig. 2), could be attributed to the partial filling of the pores by water in liquid conditions. Furthermore, we did not employ a fixed-bed of quartz beads at the column inlet or outlet, but left the dead volume open. Although a small kink in the breakthrough profile is visible at $y/y_{in} = 0.2$, possibly indicating channeling effects, these were not observed when performing a pure isobutanol vapor phase breakthrough experiment (Fig. S13). Hence, even without an aid in flow distribution, the flow appears to be reasonably distributed across the monolith in gas phase. The obtained sharp breakthrough profile indicates no large dispersion or mass transfer resistances in vapor phase conditions.

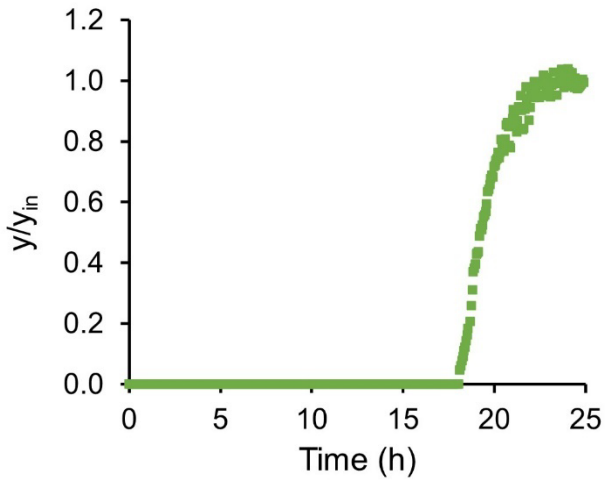

Fig. 5 Single component adsorption breakthrough curve of *n*-butanol (1856 Pa) at a flowrate of 250 NmL/min at 40 °C on the activated carbon monolith

3.6 Analysis of characteristic mass transfer times

To compare these differences between vapor and liquid phase behavior, characteristic time constants for mass transfer were estimated for the performed liquid and vapor breakthrough measurements (Eqs. 7–9). The external film resistance was estimated using the Hawthorn equation (Eq. 6), while the internal mass transfer resistance was estimated by calculating the internal diffusion coefficient via the liquid or gas phase molecular diffusion

coefficient and the slope of the *n*-butanol adsorption isotherm (Eq. S11). A comparison was made in both conditions with the average contact time of the carrier gas or liquid.

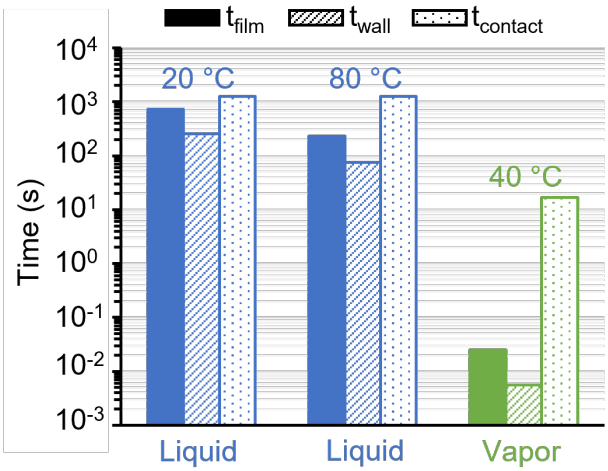

Fig. 6 Characteristic mass transfer time constants for liquid (flowrate of 3.0 mL/min) and vapor (flowrate of 250 NmL/min) phase breakthrough measurements on the monolith column

From this analysis (Fig. 6), it can be seen that in vapor conditions, the contact time of the gas is nearly 3 orders of magnitude larger than the characteristic time for external or internal mass transfer. In contrast, in liquid phase conditions, the characteristic time for film mass transfer or internal diffusion lies much closer to the contact time. For instance, at a flow rate of 3 ml/min in liquid phase, the fluid had a contact time of 1.3 10^3 s, while the characteristic time for external film resistance was equal to 7.3 10^2 s. On the other hand, for the vapor phase breakthrough experiments, the contact time of the gas is 17 s, while the characteristic time for external film resistance is only 2.5 10^{-2} s. Hence, in liquid phase conditions, the smaller diffusion coefficients lead to a much higher external film resistance than in gas phase conditions. It is hypothesized that the higher diffusivity in gas phase not only aids in the mass transfer of *n*-butanol, but also helps in distributing the flow at the column inlet.

4 Conclusion

The activated carbon monolith studied in this work shows a high equilibrium adsorption capacity for *n*-butanol in liquid phase and the crushed activated carbon is able to separate model ABE mixtures. Unfortunately, when investigating the full monolith in dynamic conditions, broad breakthrough profiles were observed. Whether this breakthrough curve broadening could be related to flow maldistribution effects or mass transfer could not be fully clarified. However, in vapor phase conditions, these flow maldistribution or mass transfer effects were not present. By comparing characteristic times for mass transfer, it was shown that the external film resistance plays a much more important role in liquid phase adsorption of *n*-butanol, compared to the vapor phase adsorption.

Competing interests

The authors have no competing interests to declare that are relevant to the content of this article.

Funding

No funding was received for conducting this study.

References

Abdehagh, N., Dai, B., Thibault, J., Handan Tezel, F.: Biobutanol separation from ABE model solutions and fermentation broths using a combined adsorption-gas stripping process. J. Chem. Technol. Biotechnol. 92, 245–251 (2017). https://doi.org/10.1002/jctb.4977

Abdehagh, N., Tezel, F.H., Thibault, J.: Adsorbent screening for biobutanol separation by adsorption: Kinetics, isotherms and competitive effect of other compounds. Adsorption. 19, 1263–1272 (2013). https://doi.org/10.1007/s10450-013-9566-8

Abdehagh, N., Tezel, F.H., Thibault, J.: Separation techniques in butanol production: Challenges and developments. Biomass and Bioenergy. 60, 222–246 (2014). https://doi.org/10.1016/j.biombioe.2013.10.003

Ahn, H., Brandani, S.: Dynamics of carbon dioxide breakthrough in a carbon monolith oiver a wide concentration range. Adsorption. 11, 473–477 (2005). https://doi.org/10.1007/s10450-005-5970-z

Akhtar, F., Andersson, L., Ogunwumi, S., Hedin, N., Bergström, L.: Structuring adsorbents and catalysts by processing of porous powders. J. Eur. Ceram. Soc. 34, 1643–1666 (2014). https://doi.org/10.1016/j.jeurceramsoc.2014.01.008

Bhattacharyya, S., Jayachandrababu, K.C., Chiang, Y., Sholl, D.S., Nair, S.: Butanol Separation from Humid CO 2 -Containing Multicomponent Vapor Mixtures by Zeolitic Imidazolate Frameworks. ACS Sustain. Chem. Eng. 5, 9467–9476 (2017). https://doi.org/10.1021/acssuschemeng.7b02604

Cao, Y., Wang, K., Wang, X., Gu, Z., Gibbons, W., Vu, H.: Adsorption of butanol vapor on active carbons with nitric acid hydrothermal modification. Bioresour. Technol. 196, 525–532 (2015). https://doi.org/10.1016/j.biortech.2015.08.027

Claessens, B., Dubois, N., Lefevere, J., Mullens, S., Cousin-Saint-Remi, J., Denayer, J.F.M.: 3D-Printed ZIF-8 Monoliths for Biobutanol Recovery. Ind. Eng. Chem. Res. 59, 8813–8824 (2020)(a). https://doi.org/10.1021/acs.iecr.0c00453

Claessens, B., De Staercke, M., Verstraete, E., Baron, G., Cousin-Saint-Remi, J., Denayer, J.F.M.: Identifying selective adsorbents for the recovery of renewable isobutanol. ACS Sustain. Chem. Eng. acssuschemeng.0c02316 (2020)(b). https://doi.org/10.1021/acssuschemeng.0c02316

Claessens, B., Wittevrongel, G.R., Rey, F., Valencia, S., Cousin-Saint-Remi, J., Baron, G. V., Denayer, J.F.M.: Capturing renewable isobutanol from model vapor mixtures using an all-silica beta zeolite. Chem. Eng. J. 412, 128658 (2021). https://doi.org/10.1016/j.cej.2021.128658

Cousin-Saint-Remi, J., Baron, G., Denayer, J.: Adsorptive separations for the recovery and purification of biobutanol. Adsorption. 18, 367–373 (2012). https://doi.org/10.1007/s10450-012-9415-1

Cousin-Saint-Remi, J., Remy, T., Vanhunskerken, V., Vandeperre, S., Duerinck, T., Maes, M., Devos, D., Gobechiya, E., Kirschhock, C.E.A., Baron, G. V., Denayer, J.F.M.: Biobutanol separation with the metal-organic framework ZIF-8. ChemSusChem. 4, 1074–1077 (2011). https://doi.org/10.1002/cssc.201100261

Crittenden, B., Patton, A., Jouin, C., Perera, S., Tennison, S., Echevarria, J.A.B.: Carbon monoliths: A comparison with granular materials. Adsorption. 11, 537–541 (2005). https://doi.org/10.1007/s10450-005-5981-9

DeWitt, S.J.A., Sinha, A., Kalyanaraman, J., Zhang, F., Realff, M.J., Lively, R.P.: Critical Comparison of Structured Contactors for Adsorption-Based Gas Separations. Annu.

Rev. Chem. Biomol. Eng. 9, 129–152 (2018). https://doi.org/10.1146/annurev-chembioeng-060817-084120

Duerinck, T., Leflaive, P., Martin, P., Pirngruber, G.D., Denayer, J.F.M.: A high-throughput methodology for liquid phase adsorption experimentation. Adsorption. 17, 347–359 (2011). https://doi.org/10.1007/s10450-011-9338-2

Dürre, P.: Biobutanol: An attractive biofuel. Biotechnol. J. 2, 1525–1534 (2007). https://doi.org/10.1002/biot.200700168

Faisal, A., Zarebska, A., Saremi, P., Korelskiy, D., Ohlin, L., Rova, U., Hedlund, J., Grahn, M.: MFI zeolite as adsorbent for selective recovery of hydrocarbons from ABE fermentation broths. Adsorption. 20, 465–470 (2014). https://doi.org/10.1007/s10450-013-9576-6

Faisal, A., Zhou, M., Hedlund, J., Grahn, M.: Recovery of butanol from model ABE fermentation broths using MFI adsorbent: a comparison between traditional beads and a structured adsorbent in the form of a film. Adsorption. 22, 205–214 (2016). https://doi.org/10.1007/s10450-016-9759-z

Faisal, A., Zhou, M., Hedlund, J., Grahn, M.: Zeolite MFI adsorbent for recovery of butanol from ABE fermentation broths produced from an inexpensive black liquor-derived hydrolyzate. Biomass Convers. Biorefinery. 8, 679–687 (2018). https://doi.org/10.1007/s13399-018-0315-9

Gao, C., Shi, Q., Dong, J.: Adsorptive separation performance of 1-butanol onto typical hydrophobic zeolitic imidazolate frameworks (ZIFs). CrystEngComm. 18, 3842–3849 (2016). https://doi.org/10.1039/C6CE00249H

Gao, C., Wu, J., Shi, Q., Ying, H., Dong, J.: Adsorption breakthrough behavior of 1-butanol from an ABE model solution with high-silica zeolite: Comparison with zeolitic imidazolate frameworks (ZIF-8). Microporous Mesoporous Mater. 243, 119–129 (2017). https://doi.org/10.1016/j.micromeso.2017.02.009

Groot, W.J., Luyben, K.C.A.M.: In situ product recovery by adsorption in the butanol / isopropanol batch fermentation. Appl. Microbiol. Biotechnol. 25, 29–31 (1986). https://doi.org/10.1007/bf00252508

Hahn, H.-D., Dämbkes, G., Rupprich, N., Bahl, H., Frey, G.D.: Butanols. Ullmann's Encycl. Ind. Chem. (2013). https://doi.org/10.1002/14356007.a04_463.pub3

Hawthorn, R.D.: Afterburner catalysts-effects of heat and mass transfer between gas and catalyst surface. (1974)

Ibrahim, M.F., Kim, S.W., Abd-Aziz, S.: Advanced bioprocessing strategies for biobutanol production from biomass. Renew. Sustain. Energy Rev. 91, 1192–1204 (2018). https://doi.org/10.1016/j.rser.2018.04.060

Jang, Y.S., Malaviya, A., Cho, C., Lee, J., Lee, S.Y.: Butanol production from renewable biomass by clostridia. Bioresour. Technol. 123, 653–663 (2012). https://doi.org/10.1016/j.biortech.2012.07.104

Jiao, P., Wu, J., Ji, Y., Ke, X., Zou, F., Zhou, J., Zhuang, W., Ying, H.: Desorption of 1-butanol from polymeric resin: experimental studies and mathematical modeling. RSC Adv. 5, 105464–105474 (2015). https://doi.org/10.1039/C5RA21986H

Kärger, J., Ruthven, D.M., Theodorou, D.N.: Diffusion in Nanoporous Materials. Wiley-VCH Verlag GmbH & Co. KGaA, Weinheim, Germany (2012)

Ku, H.H.: Notes on the use of propagation of error formulas. J. Res. Natl. Bur. Stand. Sect. C Eng. Instrum. 70C, 263 (1966). https://doi.org/10.6028/jres.070c.025

Kumar, M., Gayen, K.: Developments in biobutanol production: New insights. Appl. Energy. 88, 1999–2012 (2011). https://doi.org/10.1016/j.apenergy.2010.12.055

Kushwaha, D., Srivastava, N., Mishra, I., Upadhyay, S.N., Mishra, P.K.: Recent trends in biobutanol production. Rev. Chem. Eng. 35, 475–504 (2019). https://doi.org/10.1515/revce-2017-0041

Lee, S.H., Yun, E.J., Kim, J., Lee, S.J., Um, Y., Kim, K.H.: Biomass, strain engineering, and fermentation processes for butanol production by solventogenic clostridia. Appl. Microbiol. Biotechnol. 1–17 (2016). https://doi.org/10.1007/s00253-016-7760-9

Lefevere, J., Claessens, B., Mullens, S., Baron, G., Cousin-Saint-Remi, J., Denayer, J.F.M.: 3D-Printed Zeolitic Imidazolate Framework Structures for Adsorptive Separations. ACS Appl. Nano Mater. 2, 4991–4999 (2019). https://doi.org/10.1021/acsanm.9b00934

Levario, T.J., Dai, M., Yuan, W., Vogt, B.D., Nielsen, D.R.: Rapid adsorption of alcohol biofuels by high surface area mesoporous carbons. Microporous Mesoporous Mater. 148, 107–114 (2012). https://doi.org/10.1016/j.micromeso.2011.08.001

Li, Y.Y., Perera, S.P., Crittenden, B.D.: Zeolite Monoliths for Air Separation. Chem. Eng. Res. Des. 76, 931–941 (1998). https://doi.org/10.1205/026387698525739

Lin, X., Li, R., Wen, Q., Wu, J., Fan, J., Jin, X., Qian, W., Liu, D., Chen, X., Chen, Y., Xie, J., Bai, J., Ying, H.: Experimental and modeling studies on the sorption breakthrough behaviors of butanol from aqueous solution in a fixed-bed of KA-I resin. Biotechnol. Bioprocess Eng. 18, 223–233 (2013). https://doi.org/10.1007/s12257-012-0549-5

Lin, X., Wu, J., Fan, J., Qian, W., Zhou, X., Qian, C., Jin, X., Wang, L., Bai, J., Ying, H.: Adsorption of butanol from aqueous solution onto a new type of macroporous adsorption resin: Studies of adsorption isotherms and kinetics simulation. J. Chem. Technol. Biotechnol. 87, 924–931 (2012). https://doi.org/10.1002/jctb.3701

Liu, S.: Cooperative adsorption on solid surfaces. J. Colloid Interface Sci. 450, 224–238 (2015). https://doi.org/10.1016/j.jcis.2015.03.013

Maddox, I.S.: Use of silicalite for the adsorption of n-butanol from fermentation liquors. Biotechnol. Lett. 4, 759–760 (1982). https://doi.org/10.1007/BF00134673

Milestone, N.B., Bibby, D.M.: Concentration of alcohols by adsorption on silicalite. J. Chem. Technol. Biotechnol. 31, 732–736 (1981). https://doi.org/10.1002/jctb.503310198

Milestone, N.B., Bibby, D.M.: Adsorption of alcohols from aqueous solution by ZSM-5. J. Chem. Technol. Biotechnol. Chem. Technol. 34, 73–79 (1983). https://doi.org/10.1002/jctb.5040340205

Mosca, A., Hedlund, J., Webley, P.A., Grahn, M., Rezaei, F.: Structured zeolite NaX coatings on ceramic cordierite monolith supports for PSA applications. Microporous Mesoporous Mater. 130, 38–48 (2010). https://doi.org/10.1016/j.micromeso.2009.10.010

Nielsen, D.R., Prather, K.J.: In situ product recovery of n-butanol using polymeric resins. Biotechnol. Bioeng. 102, 811–821 (2009). https://doi.org/10.1002/bit.22109

Nielsen, L., Larsson, M., Holst, O., Mattiasson, B.: Adsorbents for extractive bioconversion applied to the acetone-butanol fermentation. Appl. Microbiol. Biotechnol. 28, 335–339 (1988). https://doi.org/10.1007/BF00268191

Oudshoorn, A., van der Wielen, L.A.M., Straathof, A.J.J.: Adsorption equilibria of bio-based butanol solutions using zeolite. Biochem. Eng. J. 48, 99–103 (2009). https://doi.org/10.1016/j.bej.2009.08.014

Van der Perre, S., Gelin, P., Claessens, B., Martin-Calvo, A., Cousin Saint Remi, J., Duerinck, T., Baron, G. V., Palomino, M., Sanchez, L.Y., Valencia, S., Shang, J., Singh, R., Webley, P.A., Rey, F., Denayer, J.: Intensified biobutanol recovery using zeolites with complementary selectivity. ChemSusChem. (2017). https://doi.org/10.1002/cssc.201700667

Poling, B.E., Prausnitz, J.M., O'Connell, J.P.: Properties of Gases and Liquids. (2007)

Qureshi, N., Blaschek, H.: Evaluation of recent advances in butanol fermentation, upstream, and downstream processing. Bioprocess Biosyst. Eng. 24, 219–226 (2001). https://doi.org/10.1007/s004490100257

Qureshi, N., Hughes, S., Maddox, I.S., Cotta, M.A.: Energy-efficient recovery of butanol from model solutions and fermentation broth by adsorption. Bioprocess Biosyst. Eng. 27, 215–222 (2005). https://doi.org/10.1007/s00449-005-0402-8

Raganati, F., Procentese, A., Olivieri, G., Russo, M.E., Salatino, P., Marzocchella, A.: Bio-butanol separation by adsorption on various materials: Assessment of isotherms and effects of other ABE-fermentation compounds. Sep. Purif. Technol. 191, 328–339 (2018). https://doi.org/10.1016/j.seppur.2017.09.059

Rezaei, F., Grahn, M.: Thermal management of structured adsorbents in CO 2 capture processes. Ind. Eng. Chem. Res. 51, 4025–4034 (2012). https://doi.org/10.1021/ie201057p

Rezaei, F., Webley, P.: Optimum structured adsorbents for gas separation processes. Chem. Eng. Sci. 64, 5182–5191 (2009). https://doi.org/10.1016/j.ces.2009.08.029

Rezaei, F., Webley, P.: Structured adsorbents in gas separation processes. Sep. Purif. Technol. 70, 243–256 (2010). https://doi.org/10.1016/j.seppur.2009.10.004

Ruthven, D.M.: Principles of adsorption and adsorption processes. John Wiley & Sons, New York (1984)

Saravanan, V., Waijers, D.A., Ziari, M., Noordermeer, M.A.: Recovery of 1-butanol from aqueous solutions using zeolite ZSM-5 with a high Si/Al ratio; suitability of a column process for industrial applications. Biochem. Eng. J. 49, 33–39 (2010). https://doi.org/10.1016/j.bej.2009.11.008

Sharma, I., Mennitto, R., Friedrich, D., Brandani, S.: Combining the Nonuniform Structure and Flow Maldistribution for the Accurate Prediction of the Process Performance of Monolithic Adsorbent Systems. Ind. Eng. Chem. Res. 59, 3162–3172 (2020). https://doi.org/10.1021/acs.iecr.9b05845

Staggs, K.W., Nielsen, D.R.: Improving n-butanol production in batch and semi-continuous processes through integrated product recovery. Process Biochem. 50, 1487–1498 (2015). https://doi.org/10.1016/j.procbio.2015.06.009

Staggs, K.W., Qiang, Z., Madathil, K., Gregson, C., Xia, Y., Vogt, B., Nielsen, D.R.: High Efficiency and Facile Butanol Recovery with Magnetically Responsive Micro/Mesoporous Carbon Adsorbents. ACS Sustain. Chem. Eng. 5, 885–894 (2017). https://doi.org/10.1021/acssuschemeng.6b02204

Tashiro, Y., Yoshida, T., Noguchi, T., Sonomoto, K.: Recent advances and future prospects for increased butanol production by acetone-butanol-ethanol fermentation. Eng. Life Sci. 13, 432–445 (2013). https://doi.org/10.1002/elsc.201200128

Weizmann, C., Bergmann, E., Sulzbacher, M., Pariser, E.R.: Studies in selective extraction and adsorption. III. The adsorption of acetone, butyl alcohol and 2:3-butylene glycol from dilute solutions. J. Soc. Chem. Ind. 67, 225–227 (1948). https://doi.org/10.1002/jctb.5000670604

Wu, J., Zhuang, W., Ying, H., Jiao, P., Li, R., Wen, Q., Wang, L., Zhou, J., Yang, P.: Acetone-butanol-ethanol competitive sorption simulation from single, binary, and ternary systems in a fixed-bed of KA-I resin. Biotechnol. Prog. 31, 124–134 (2015). https://doi.org/10.1002/btpr.2019

Xue, C., Liu, F., Xu, M., Tang, I.C., Zhao, J., Bai, F., Yang, S.T.: Butanol production in acetone-butanol-ethanol fermentation with in situ product recovery by adsorption. Bioresour. Technol. 219, 158–168 (2016). https://doi.org/10.1016/j.biortech.2016.07.111

Yang, X., Tsai, G.J., Tsao, G.T.: Enhancement of in situ adsorption on the acetone-butanol fermentation by Clostridium acetobutylicum. Sep. Technol. 4, 81–92 (1994). https://doi.org/10.1016/0956-9618(94)80009-X